

Article

Nylon-6-Coated Doxorubicin-Loaded Magnetic Nanoparticles and Nanocapsules for Cancer Treatment

Ekaterina Kovrigina ¹, Yuliya Poletaeva ¹, Yanfang Zheng ², Alexey Chubarov ^{1,*} and Elena Dmitrienko ^{1,*}¹ Institute of Chemical Biology and Fundamental Medicine SB RAS, 630090 Novosibirsk, Russia,² Affiliated Cancer Hospital & Institute of Guangzhou Medical University, Guangzhou 510095, China

* Correspondence: chubarov@niboch.nsc.ru or chubarovalesha@mail.ru (A.C.); elenad@niboch.nsc.ru (E.D.); Tel.: +7-913-763-1420 (A.C.); +7-913-904-17-42 (E.D.)

Abstract: Nanoplatfoms used for the loading of anticancer drugs constitute a promising approach to cancer treatment and reducing the side effects of these drugs. Among the cutting-edge systems used in this area are magnetic nanocomposites (MNCs) and nanocapsules (NCs). MNCs are considered to constitute a smart tool for magnetic-field-guided targeted drug delivery, magnetic resonance imaging, and hyperthermia therapy. Nanocapsules offer great potential due to their ability to control drug-loading capacity, their release efficiency, their stability, and the ease with which their surfaces can be modified. This study proposes a method for the development of nylon-6-coated MNCs and nylon-6 polymeric membrane NCs. A biocompatible nylon-6 polymer was first used for NC synthesis. Oleic-acid-modified and non-modified Fe₃O₄ nanoparticles were synthesized for the production of nylon-coated MNCs. Dynamic light scattering (DLS), transmission electron microscopy (TEM), and ζ-potential measurements were used to perform size, morphology, and charge analyses. The above-mentioned two types of MNCs were considered templates for the manufacture of nylon nanocapsules, leading to NCs with different charges and structures. The developed oleic-acid-coated nylon-6 MNCs and NCs showed excellent loading values of the chemotherapy drug doxorubicin (DOX) of up to 732 and 943 μg/mg (DOX/MNC or NC), respectively. On the contrary, the capacity of the nano-construction that was not modified with oleic acid did not exceed 140 μg/mg. The DOX-loaded nanosystems displayed pH-sensitive drug release properties, for which the highest efficiency was observed at an acidic pH. The series of DOX-loaded MNCs and NCs inhibited A549 and HEK 293FT cell lines, with the lowest IC₅₀ value of 0.31 μM observed for the nanocapsules, which is a 1.5-fold lower concentration than the free DOX. Therefore, the presented nanoscale systems offer great potential for cancer treatment.

Keywords: iron oxide nanoparticles; nylon 6; nanocapsules; polymer nanocomposites; doxorubicin; coatings; pH stimuli response; drug delivery; toxicity; cancer treatment



Citation: Kovrigina, E.; Poletaeva, Y.; Zheng, Y.; Chubarov, A.; Dmitrienko, E. Nylon-6-Coated Doxorubicin-Loaded Magnetic Nanoparticles and Nanocapsules for Cancer Treatment. *Magnetochemistry* **2023**, *9*, 106. <https://doi.org/10.3390/magnetochemistry9040106>

Academic Editor: Alejandro Gómez Roca

Received: 28 February 2023

Revised: 6 April 2023

Accepted: 10 April 2023

Published: 12 April 2023



Copyright: © 2023 by the authors. Licensee MDPI, Basel, Switzerland. This article is an open access article distributed under the terms and conditions of the Creative Commons Attribution (CC BY) license (<https://creativecommons.org/licenses/by/4.0/>).

1. Introduction

Cancer is considered one of the most frequently occurring diseases in the world [1]. However, cancer treatment drugs have numerous side effects that arise from non-specific delivery and subsequent strong damage to healthy organs and cells. Doxorubicin (DOX) is a widely used anthracycline antibiotic applied in many types of cancers [2–6]. The mechanism of DOX activity includes DNA intercalation and strand disruption, topoisomerase II inhibition, the formation of iron or copper metal complexes, and reactive oxygen species formation [2]. Unfortunately, DOX-assisted therapy is associated with drug resistance and numerous side effects for the entire body [4,5]. These toxic effects comprise cyto-, cardio-, and myelotoxicity; headaches; nausea; and so on. Moreover, DOX has poor solubility and tends to aggregate, leading to the creation of fibril-like structures [6]. The recent developments in this field focus on the manufacture of DOX-loaded nanocomposites, which have effectively been used for targeted delivery and efficient drug release in cancer tissue [7–15].

However, efficient vehicle design for effective therapeutic drug delivery poses a significant challenge in clinical cancer treatment. Various nanoscale systems based on polymers, gold, calcium carbonate, silica, magnetic materials, biological components, or bioinspired have been proposed as controlled release methods for DOX [7–21].

Well-tuned nano-constructions may accumulate in solid tumors due to their enhanced permeation and retention effect, which allow them to retain large-sized structures in the nutritional gap. The particles should be greater than 15–20 nm and lower than 150 nm. Particles smaller than 15 nm are removed from the blood through the kidneys, while those higher than 150 nm are absorbed by the liver and spleen and pose problems with vascular structures' penetration and cellular internalization. By combining nanotechnology and responsive DOX delivery systems, various nanocomposites can be synthesized, thus avoiding drug resistance problems [8,13,16,21].

Magnetic nanocomposites (MNCs) have widespread applications in magnetic resonance imaging, hyperthermia therapy, and theranostics [18,22–39]. MNCs based on Fe₃O₄ nanoparticles (MNPs) provide ferromagnetic properties suitable for magnetically targeted anticancer drugs and gene delivery [1,13,40–48]. MNCs offer many advantages, including high stability, low toxicity, good biocompatibility, and easy functionalization. However, in most cases, the magnetic core should be completely protected by various organic and inorganic materials. One of the popular approaches to achieve this is polymer coating [13,49–54]. A wide range of polymers and their functional groups provide excellent diversification of colloidal stability, charge, solubility in water, salt and temperature stability, viscosity, and further modification by address or reporter groups [13,49–60].

Nylon is a versatile polyamide polymer that has found several biomedical applications due to its excellent mechanical and physical properties [61]. Nylon-6 is widely used for the manufacture of medical materials [18,61–63]. Nylon exhibits high chemical stability, amphiphilic properties, and excellent biocompatibility [16,61]. Due to its low density and ability to aggregate, nylon may form extensive porous structures, which may be a promising affordance in terms of drug loading [16,18,61].

Polymer-coated MNCs may be transformed into nanocapsules (NC) by destroying their magnetic cores in extremely acidic media [64,65]. NCs are nanoshells consisting of a polymeric membrane and a liquid core. NCs have unique properties that make them attractive for bio-applications [64,66]. The encapsulation of an anticancer drug into an NC can reduce its toxic effects and provide controlled release in a desired location [65,67–73]. Targeted delivery and controlled drug release from MNCs and NCs increase the effectiveness and reduce the side effects of chemotherapy.

Controlled drug release in a cancer tissue environment by a pH-stimuli-response is a well-known method with high prospects in this field [8,13,16,21]. pH-responsive constructions should have extremely low drug release properties in plasma (pH~7.4) and healthy tissue. On the contrary, composites should have efficient drug release properties at pH~5 in a tumor, which is a level that can be found in a tumor's extracellular matrix [74–79].

Herein, we report the synthesis of pH-stimuli-sensitive, DOX-loaded, nylon-modified, oleic-acid-coated, or non-coated MNCs and NCs. Two types of magnetic nanoparticles with and without oleic acid surfactants were used as cores for the manufacture of further composites. Nylon-6 polymer was first used as an MNP coating for drug delivery and as an NC membrane. The synthesized oleic-acid-coated or non-coated MNCs and NCs provided different charges and morphologies, which strongly influenced drug capacity and pH-sensitive release. The oleic-acid- and nylon-6-coated MNCs and NCs showed an excellent DOX-loading capacity of up to 732 and 943 µg/mg (DOX/MNC or NC), respectively. On the contrary, the non-modified-with-oleic-acid nano-constructions' capacity did not exceed 140 µg/mg. The pH-sensitive DOX release profile of the constructions was estimated, for which it was determined that they had highly efficient levels of drug release at an acidic pH. The prospective effects of the DOX-loaded MNCs and NCs were shown on A549 and HEK 293FT cell lines. The excellent capacity, efficient drug release in acidic media, and high cancer cell inhibition observed exhibit the promising potential of the

DOX-loaded nylon-based NCs synthesized from oleic-acid-modified MNCs for the field of drug-resistance therapeutics.

2. Results and Discussion

2.1. Synthesis and Characterization of MNPs

MNPs and oleic-acid-coated MNPs (MNP_OA) were synthesized according to previously published procedures via classical co-precipitation methods [13,18,80]. MNPs and MNP_OA have similar sizes but opposite particle charges (Table 1). In comparison to MNPs, the MNP_OA has a ζ -potential of -43 mV, usually indicating perfect colloidal stability. Oleic acid (OA) was used as a primary surfactant for surface stabilization, which is necessary for making monodisperse and uniform MNPs [81,82]. Moreover, the presence of OA with a negatively charged carboxylic group transforms the nanoparticles' positive charge to a negative one (Table 1, cf. MNP and MNP_OA).

Table 1. DLS data for MNP and MNP_OA.

NP Type	Hydrodynamic Diameter, nm	Polydispersity Index	ζ -Potential, mV
MNP	123 ± 7	0.205 ± 0.005	23.0 ± 8.0
MNP_OA	112 ± 18	0.172 ± 0.010	-43.0 ± 0.9

To endow the MNPs and MNP_OA with better colloidal stability, the presence of 0.05–0.1% Tween 20 in mQ water during storage and TEM analysis is required. Tween is a non-ionic amphiphilic surfactant that consists of a polar head and a hydrophobic alkyl chain, thus providing better water solubility [51,83]. The TEM results are shown in Figure 1. Nanoparticles with a size of ~ 13 nm form clusters up to 100–150 nm in both cases (Figure 1).

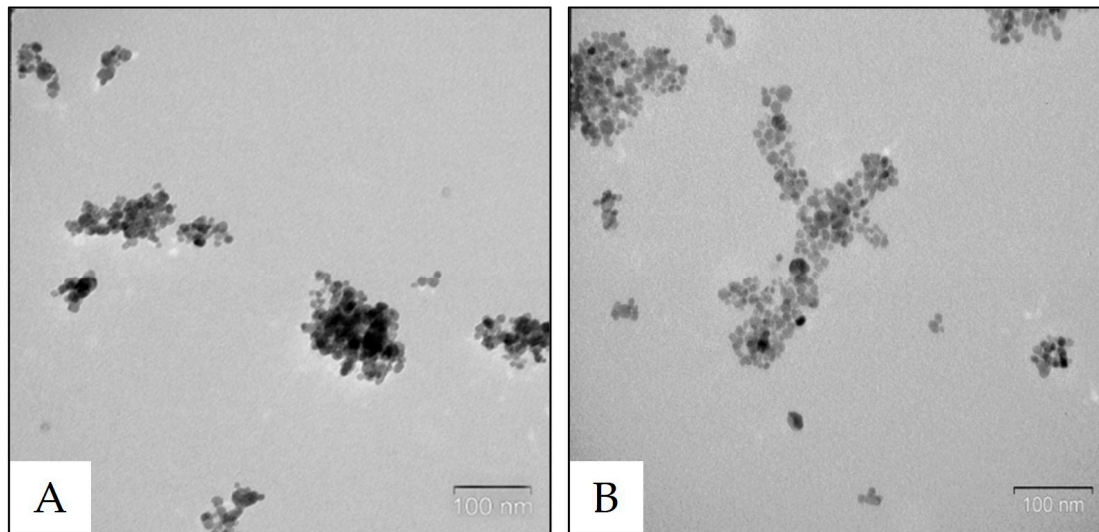


Figure 1. TEM images of MNP (A) and MNP_OA (B). The bar indicates 100 nm.

2.2. Nylon-6-Coated Nanocomposites' Synthesis

The nanocomposites were obtained according to a four-step procedure (Figure 2). Their synthesis was carried out according to a procedure that was previously developed by the authors [16,18] consisting of the widely used tetraethyl orthosilicate/3-aminopropyltriethoxysilane (TEOS/APTES) method [84–90] with a subsequent 2,4,6-trichloro-1,3,5-triazine reaction. The activated surface of the MNPs may be further modified with nylon-6 polymer [16,18]. The nanocapsules (NC1 and NC2) were obtained via magnetic core destruction using a strong acid. NC1 and NC2 were synthesized from MNP_Ny and MNP_OA_Ny, respectively. To confirm the components of the MNCs and NCs, the FT-IR spectra of the MNP_OA, MNP_OA_Ny, and NC2 were recorded, and the results are presented in Figure 3. The

FT-IR spectrum of the MNP_OA provides the characteristic peaks of OA at 2918 cm^{-1} , 2837 cm^{-1} (asymmetric and symmetric $-\text{CH}_2$ and $-\text{CH}_3$ stretch, respectively), 1707 cm^{-1} ($-\text{C}=\text{O}$ asymmetric stretch), 1533 cm^{-1} , 1441 cm^{-1} ($-\text{COO}$ asymmetric and symmetric stretch), 1417 cm^{-1} (CH_3 umbrella), the magnetite MNPs' core peak at 571 cm^{-1} ($\text{Fe}-\text{O}$ stretch), and water OH stretching or O-H on the MNPs' surface at 1630 cm^{-1} and 3375 cm^{-1} [21,91–96].

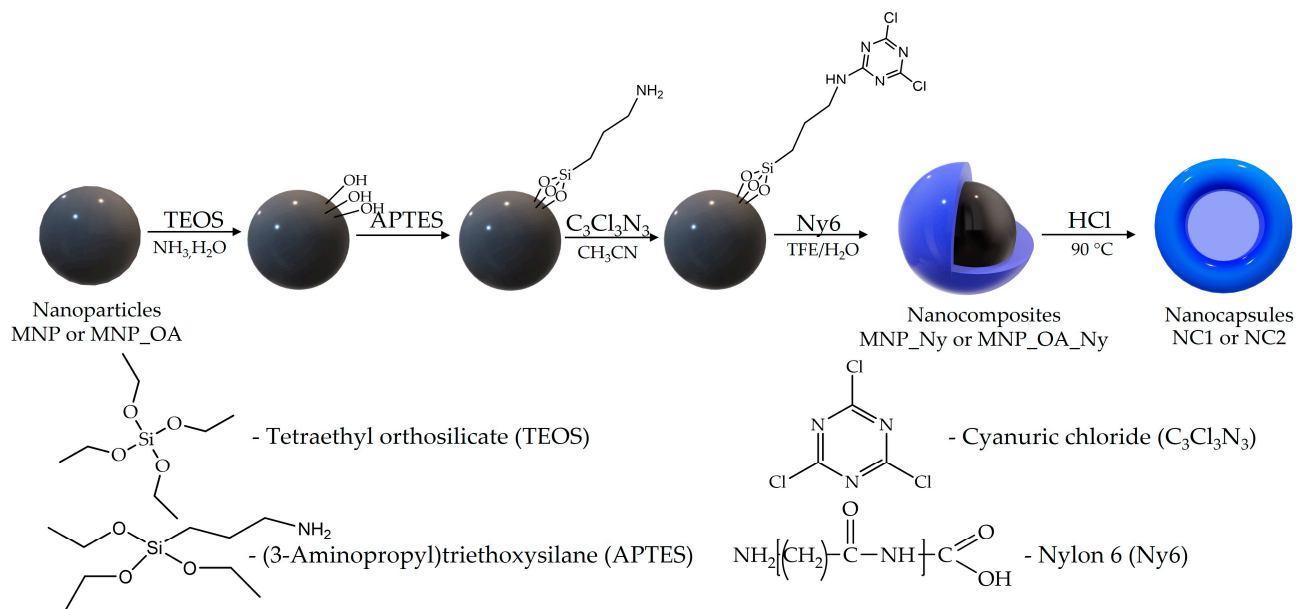


Figure 2. Schematic representation of magnetic nanocomposites' and nanocapsules' synthesis via widely used TEOS/APTES approach. TTE—trifluoroethanol.

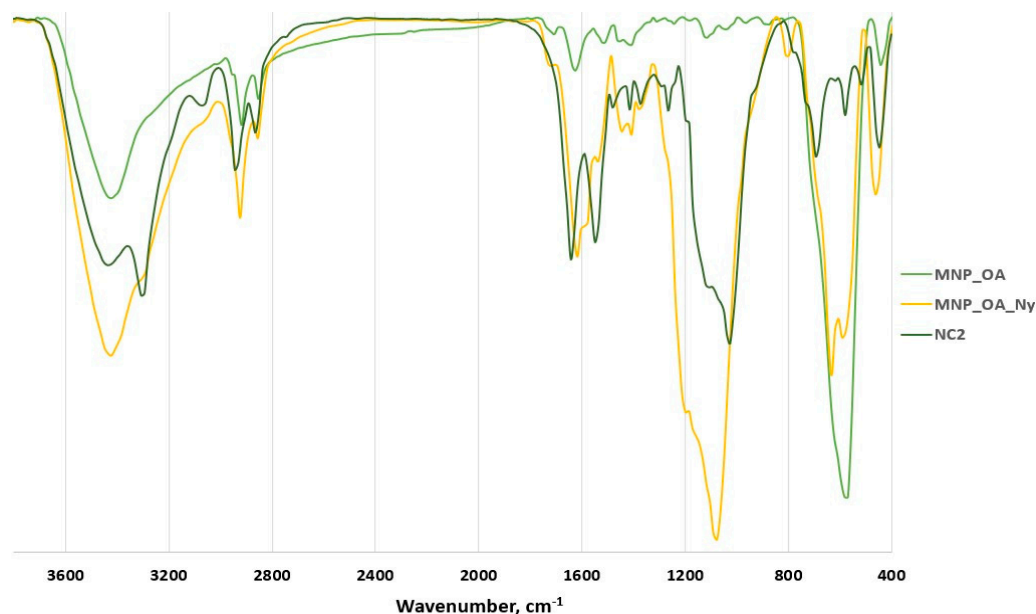


Figure 3. FT-IR spectra of MNP_OA, MNP_OA_Ny, and NC2 composites.

To confirm the successful functionalization of the MNP_OA by nylon and the nanocapsules' formation, the FT-IR spectra of MNP_OA_Ny and NC2 were recorded. The FT-IR spectrum of the NC2 nanoparticles is similar to that of pure nylon 6 (Figure 3, see <https://spectra.chem.ut.ee/textile-fibres/polyamide/>, accessed on 1 February 2023). The characteristic peaks of nylon were found at 447 , 517 , 580 ($\text{C}-\text{C}$ deformation), 694 ($\text{C}-\text{C}$ bending), 1265 ($\text{C}-\text{N}$, $\text{N}-\text{H}$), 1373 (CH_2 wagging), 1414 (CH_2 scissors, $\text{N}-\text{H}$ deformation),

1549 (C-N, N-H), 1643 (amide C = O stretch), 2864 (CH₂ symmetric stretch), 2945 (CH₂ asymmetric stretch), 3057 (N-H overtone), 3294 (N-H stretch), and 3442 cm⁻¹ (O-H and N-H stretch) [97–99]. The major peak of the silica coating at ~1026 cm⁻¹ (asymmetric Si-O-Si stretch) was also found. For MNP_OA_Ny, the characteristic peaks of silica coating were easily found at 463, 812 cm⁻¹ (symmetric Si-O-Si stretch), and 1092 cm⁻¹ [16,100,101]. The 1400–1700 cm⁻¹ area corresponds to a combination of two nylon major peaks and the O-H bending of water molecules at ~1630 cm⁻¹. The MNPs' core peak at 584 cm⁻¹ (Fe-O stretch) [91,92] splits due to mixing with nylon signals. As the characteristic peaks of nylon overlap with those of the MNPs and silica, a qualitative reaction with a N-(2-hydroxyethyl)-phenazinium ion was carried out for MNP_OA and MNP_OA_Ny [16,102]. A violet-colored product was formed by the MNP_OA_Ny (Figure S1).

Changes in the charges and sizes studied by TEM and DLS are presented in Table 2 and Figure 4. The resulting MNP_Ny and NC1 have a charge similar to that of the initial MNPs. The ζ -potentials of the MNP_Ny and NC1 are similar to the MNPs and were estimated as ranging from 25–27 mV, which indicates moderate electrostatic stability in solution. However, the particle size determined by DLS increased two-fold in comparison to that of the initial MNPs (Table 2). The MNP_Ny composite forms 201 ± 3 nm sized agglomerates as determined by DLS, which can be also seen by TEM (Figure 4A). The PDI index is about 0.3, which indicates a non-monodisperse system with small nanocomposites (~20 nm) and large agglomerates (~200–300 nm) as determined by TEM.

Table 2. DLS data for MNP_Ny, MNP_OA_Ny, NC1, and NC2.

NP Type	Hydrodynamic Diameter, nm	Polydispersity Index	ζ -Potential, mV
MNP	123 ± 7	0.205 ± 0.005	23.0 ± 8.0
MNP_Ny	201 ± 3	0.290 ± 0.021	25.0 ± 4.0
NC1	243 ± 20	0.312 ± 0.009	27 ± 5
MNP_OA	112 ± 18	0.172 ± 0.010	−43.0 ± 0.9
MNP_OA_Ny	163 ± 6	0.167 ± 0.020	−7.0 ± 0.2
NC2	130 ± 13	0.189 ± 0.012	−6.8 ± 0.3

NC1 assumes an “erythrocyte” shape upon drying, with a less electron-dense interior and an increasing shell density towards the edges (Figure 4B). NC1's thick nylon-6 membrane of ~4 nm in width was easily captured by TEM. However, both NC1 and the MNP_Ny form large agglomerates (Figure 4B). The formation of such structures can significantly affect their drug-loading properties due to the changes in the accessible surface area.

The sizes of MNP_OA_Ny and NC2 were determined to be 163 nm and 130 nm via DLS, respectively (Table 2). NC2 generates a less pronounced composite shell with low electron density and a size of 28 ± 4 nm as determined by TEM (Figure 4D). Unlike NC1, NC2 forms separate nanocapsules without aggregates, which may provide unhindered DOX loading (Figure 4D). The ζ -potential of MNP_OA_Ny and NC2 is about −7.0 mV, which primarily indicates low electrostatic stability. However, the ζ -potential of the initial MNP_OA was −43 mV. Furthermore, we did not obtain significant differences in colloidal stability between MNP_Ny and MNP_OA_Ny and NC1 and NC2, respectively. On the contrary, according to the solution behavior, MNP_OA_Ny possesses similar or better colloidal stability. A ζ -potential value lower than −30 mV and higher than +30 mV is primarily considered to correspond to sufficient physical colloidal stability. In practice, ζ -potential is not a directly measurable function. The results are highly dependent on the electrokinetic model employed [103]. We have used the Smoluchowski equation, which is the one most widely used for NPs. We assumed that phenomena such as the NPs' different sizes, various layer charges, or double-layer polarization could reduce the magnitude of the ζ -potential [103]. Moreover, for magnetite, the Smoluchowski model provides the lowest ζ -potential magnitude [103]. Due to the complex structure and different charges of the coating layers of MNP_OA_Ny and NC2, further investigation is required to fully

understand their mechanisms. Nevertheless, the MNCs and NCs match the optimal values for biomedical applications and may be used for further investigations.

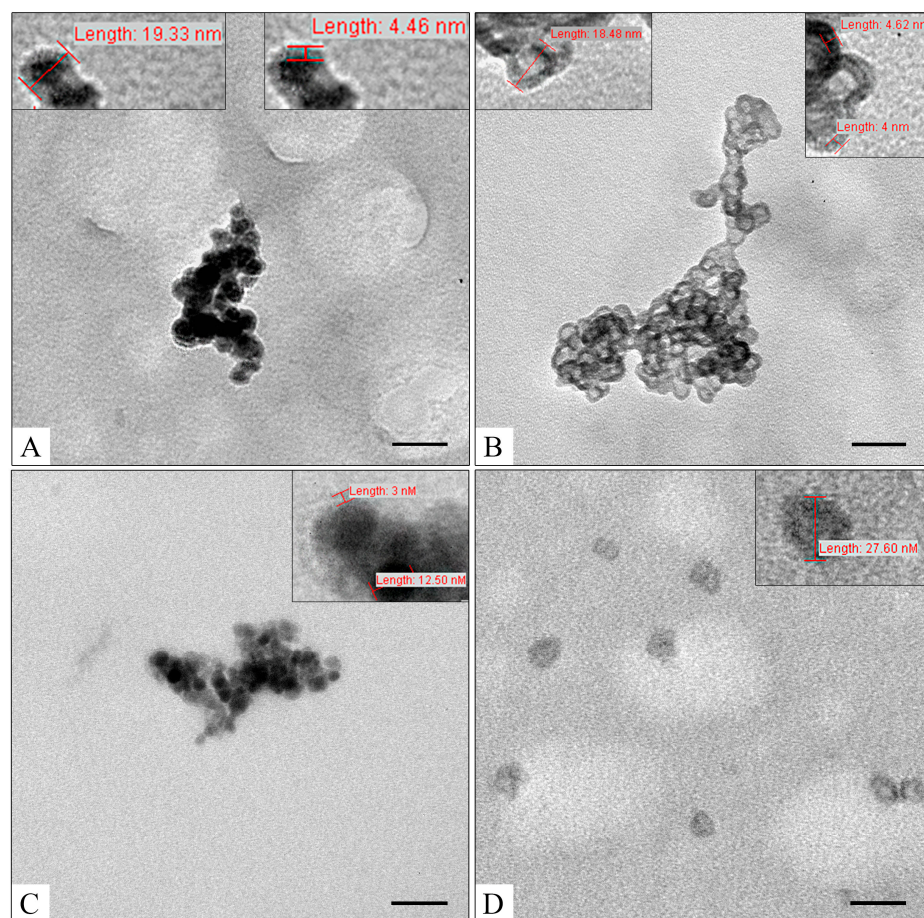


Figure 4. TEM images of MNP_Ny (A), NC1 (B), MNP_OA_Ny (C), and NC2 (D). The bar indicates 50 nm.

2.3. Anticancer Drug Doxorubicin Loading

Doxorubicin (DOX, 1 mg/mL) was loaded onto MNCs or NCs (1 mg) in 1 mL of a 10 mM sodium borate buffer (pH 8.5) (Figure 5) [13]. DOX loading was studied using UV-vis spectroscopy. The amount of drug was estimated as the difference between the added DOX and the DOX remaining in the solution after incubation with MNCs or NCs. Capacity and loading efficiencies are presented in Table 3.

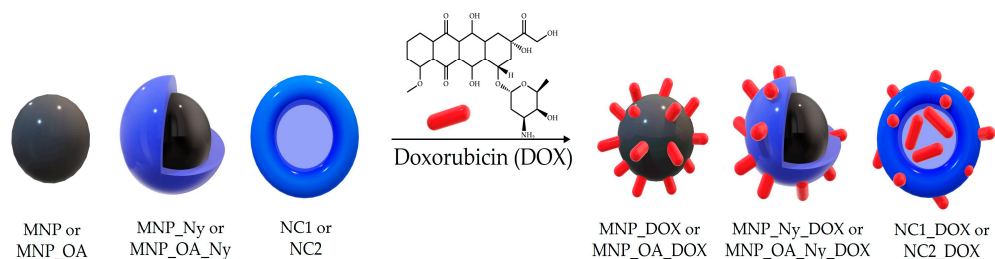


Figure 5. Schematic representation of DOX loading.

Table 3. DOX-loading capacity and loading efficiency.

Sample	DOX/MNC or NC, $\mu\text{g}/\text{mg}$	DOX-Loading Efficiency, % ¹
MNP	2 ± 1	0.4
MNP_Ny	139 ± 16	27.8
NC1	128 ± 6	25.6
MNP_OA	868 ± 37	86.8
MNP_OA_Ny	732 ± 25	73.2
NC2	943 ± 15	94.3

¹ DOX-loading efficiency = DOX in the solution after loading/initial amount of DOX; 1 mL of DOX solution (1 mg/mL) per 1 mg of MNPs was used.

OA-coated and non-modified-with-OA MNCs and NCs have extremely different DOX capacities (Table 3). The OA-coated nylon-6 MNCs and NCs show excellent DOX-loading values of up to 732 and 943 $\mu\text{g}/\text{mg}$ (DOX/MNC or NC), respectively. On the contrary, the non-modified with OA nanoconstruction's capacity does not exceed 140 $\mu\text{g}/\text{mg}$. A high capacity is associated with a good porous spatial structure of the nanosystems. Hence, OA is an essential factor in terms of nanocomposites' properties that influences drug release, delivery, and further therapeutic effects. The use of OA as a capping agent resulted in a partly hydrophobic coating and polar carboxyl groups with a negative charge (see ζ -potential, Table 2). It provides a strongly bonded protective monolayer that enhances the colloidal stability, dispersion, and crystallinity of the MNCs [13,21,104]. On the contrary, DOX has a positively charged NH_2 group and fatty aromatic rings. The presence of OA on the surface of MNPs can greatly enhance DOX capacity, leading to increased cell death [13,16,21]. Overall, the interaction between OA and DOX is complex and requires careful consideration during the development of new anticancer constructions.

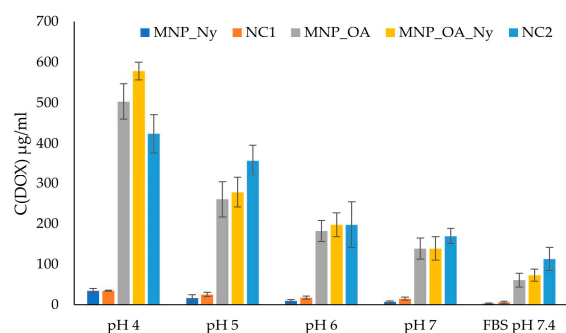
Nylon does not have any specific interactions with DOX. Nevertheless, it highly influences the DOX loading. For example, in comparison to MNPs, the DOX capacity for MNP_Ny highly increases (Table 3). Nylon 6 presents amphiphilic properties with a hydrocarbon chain and polar amide group, which may favor DOX sorption via hydrophobic and hydrogen interactions. The physical interaction between nylon and DOX can have important implications for the efficacy and safety of chemotherapy treatment. For the pair MNP_OA and MNP_OA_Ny, nylon coating slightly decreases the drug capacity, which may be associated with preferable ionic interactions instead of a hydrogen bond between DOX and a surface. In summary, the interaction between DOX and MNP_OA_Ny is complex and requires further research to fully understand. However, both the OA and nylon approaches hold promise with respect to improving the delivery and effectiveness of chemotherapy drugs such as DOX. NC2 possesses the highest capacity of 943 $\mu\text{g}/\text{mg}$ among the studied nanocomposites.

2.4. Doxorubicin Release

pH-responsive drug release is an essential feature of nano-constructions. In this study, the developed nano-constructions' DOX release efficiency was studied at pH values from 4 to 7.4. FBS solution (pH 7.4) was chosen to mimic plasma-like conditions. pH ~ 5 can be found in cell endosomes and cancer tissue. A good pH-responsive drug system should be stable at neutral pH and have efficient DOX release in acidic media for cancer treatment. The concentration of the released DOX was determined by absorption at 480 nm using a calibration curve (Figure S2). Table 4 and Figure 6 provide pH-dependent drug release data. The DOX-loaded MNCs and NCs tend to present non-efficient percentages of DOX release at neutral pH. Moreover, in acidic media, the level of drug release was more efficient, which correlates well with previously published papers [13,16,21]. Furthermore, the OA-coated nanosystems showed more efficient drug release. For example, MNP_OA_DOX, MNP_OA_Ny_DOX, and NC2_DOX showed more than 58%, 79%, and 45% drug release values, respectively, for 3 h at pH 4.0. On the contrary, without OA, MNP_Ny_DOX and NC1_DOX provide only 25–27% DOX release at pH 4.0.

Table 4. DOX release efficacy after 3 h incubation in percentages.

Sample	DOX/MNC or NC, µg/mg	Release Efficiency (%) at Various pH				
		4	5	6	7	7.4 (FBS)
MNP	2 ± 1	-	-	-	-	-
MNP_Ny	139 ± 16	25 ± 9	12 ± 2	7 ± 2	5 ± 1	2 ± 1
NC1	128 ± 6	27 ± 4	20 ± 3	14 ± 3	12 ± 2	5 ± 2
MNP_OA	868 ± 37	58 ± 5	30 ± 3	21 ± 3	16 ± 2	7 ± 3
MNP_OA_Ny	732 ± 25	79 ± 8	38 ± 4	27 ± 4	19 ± 2	10 ± 2
NC2	943 ± 15	45 ± 4	38 ± 9	21 ± 2	18 ± 3	12 ± 3

**Figure 6.** DOX release results after 3 h incubation at various pH and in FBS (pH 7.4).

The highly drug-loaded MNP_OA_DOX, MNP_OA_Ny_DOX, and NC2_DOX nanocomposites showed efficient DOX release, in terms of both absolute values (Figure 6) and percentages (Table 4), for the initial drug amount at pH 4–5. At pH 5, NC2_DOX provides the same drug release percentage as MNP_OA_Ny_DOX. However, the absolute DOX value is slightly higher for NC2_DOX. Thus, NC2_DOX shows pH-dependent drug release characteristics and is the most promising among the studied nano-constructions. Drug release presented as a function of time for the most promising NC2 is presented in Figure S3, which indicates the gradual release of the drug from the construct. An example of the DOX-loaded NC2's time-dependent drug release UV–vis spectra at pH 6 is presented in Figure S4. In comparison with NC1, NC2 has an up to seven-fold higher DOX capacity. Compared to NC1-DOX, NC2_DOX has a two-fold higher drug release efficiency of 45% at pH 4.0. Further research is needed to fully understand the nature and extent of the differences between NC1's and NC2's interaction mechanisms to develop strategies with which to enhance their effectiveness. However, a clearly observable structural difference between NC1 and NC2 (cf. Figure 4B,D) comes from the different properties of the MNPs and MNP_OA. Overall, OA can interact with nylon 6, thereby changing the MNCs' layer structure and yielding diverse sizes, charges, and morphologies (Figure 4A,C, Table 2). Moreover, a much higher NC2 drug capacity may be associated with a negative charge instead of a positive NC1. As stated above, a positively charged DOX will bind more effectively with negative-charged nanosystems. These interactions can ultimately enhance the capacity and change the pH release profile of the synthesized nanocapsules.

2.5. Cytotoxicity Studies of MNCs and NCs and DOX-Loaded Nanosystems

A cytotoxicity analysis was carried out via a widely used 3-[4,5-dimethylthiazol-2-yl]-2,5-diphenyl-tetrazolium bromide (MTT) assay (see Supplementary Materials). The lung adenocarcinoma A549 and human embryonic kidney HEK 293FT cell lines were chosen to investigate the prospects of the nano-constructions. No significant degree of cytotoxicity was obtained for the synthesized nanocomposites at up to 27 µg/mL concentration (Figure 7). The results correlate well with the previously obtained data for MNP_OA [13]. NC2 showed the highest cell viability among the studied nanosystems, which indicates the potential of these nylon capsules for drug delivery.

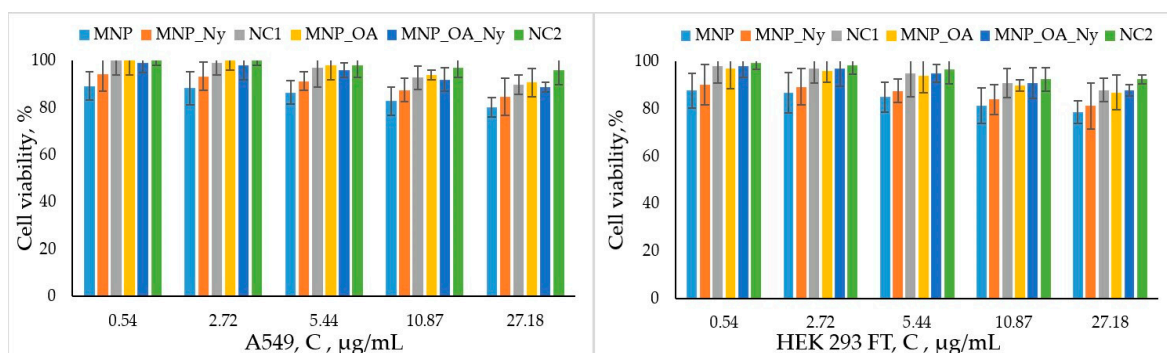


Figure 7. Cell viability assay. Cell lines A549 and HEK 293FT were incubated for 48 h with MNCs and NCs. Cells treated with PBS buffer were used as a 100% viability control. All values are given as mean \pm standard deviation (SD) values. All measurements were repeated no fewer than three times.

Various quantities of the DOX-loaded nanocomposites per drug concentration were incubated with the cells for 72 h (Figure 8). The OA-coated nanocomposites showed better cancer cell inhibition compared to free DOX, MNP_Ny_DOX, and NC1_DOX. Moreover, NC2_DOX provides the best results with respect to both the A549 and HEK 293FT cell lines. For the A549 cells, 2 μ M per DOX concentration of NC2_DOX is enough to obtain a degree of cell viability lower than 20%, which presents the successful outcome of the approach employing nylon nanocapsules.

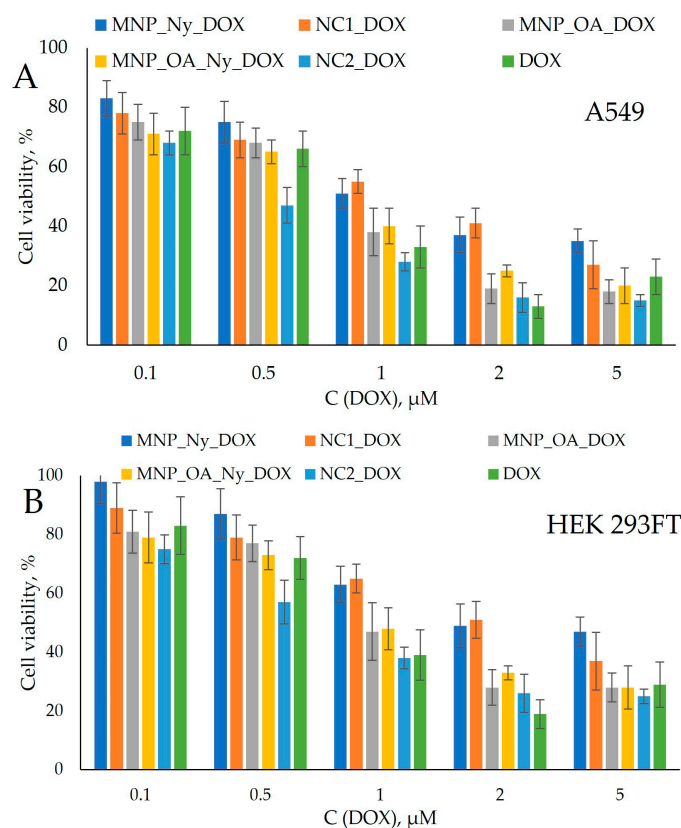


Figure 8. Cell viability assay. Cell lines A549 (A) and HEK 293FT (B) were incubated for 48 h with MNP_Ny_DOX, NC1_DOX, MNP_OA_DOX, MNP_OA_Ny_DOX, NC2_DOX, and DOX. Cells treated with PBS buffer were used as a 100% viability control. All values are given as mean \pm standard deviation (SD) values. All measurements were repeated no fewer than three times.

The half-maximum inhibitory concentration (IC50) values' recalculations are presented in Table 5. MNP_Ny_DOX and NC1_DOX yielded two-fold higher IC50 values than free DOX. On the contrary, NC2_DOX requires an almost 1.5-fold lower amount compared to the free drug to reach the necessary concentration, which ensures the death of 50% of the cells. The obtained results demonstrate the high therapeutic potential of NC2 and NC2_DOX for cancer treatment.

Table 5. The IC50 values of DOX-loaded nanocomposites and nanocapsules for A549 and HEK 293FT cell lines.

Sample	A549	HEK 293FT
	μM	μM
MNP_Ny_DOX	1.36 ± 0.08	3.09 ± 0.07
NC1_DOX	1.17 ± 0.05	2.42 ± 0.05
MNP_OA_DOX	0.60 ± 0.03	0.99 ± 0.04
MNP_OA_Ny_DOX	0.59 ± 0.02	1.01 ± 0.02
NC2_DOX	0.31 ± 0.01	0.57 ± 0.01
DOX	0.50 ± 0.04	0.79 ± 0.03

3. Materials and Methods

3.1. Materials

The $\text{FeCl}_2 \cdot 4\text{H}_2\text{O}$ used in this study was obtained from Acros organics (MW = 198.81, 99+%, Geel, Belgium). $\text{FeCl}_3 \cdot 6\text{H}_2\text{O}$ was purchased from PanReac AppliChem (MW = 270.32, 97–102%, Darmstadt, Germany). 2,4,6-Trichloro-1,3,5-triazine was obtained from Merck (Darmstadt, Germany). Nylon 6 (Product No. 181110); tetraethyl orthosilicate; (3-aminopropyl)triethoxysilane; 2,2,2-trifluoroethanol; N,N-dimethylformamide; Tween 20; oleic acid; and all solvents and reagents were purchased from Sigma (St. Louis, MO, USA) at the highest available grade and were used without purification. MTT (3-[4,5-dimethylthiazol-2-yl]-2,5-diphenyl-tetrazolium bromide) assay kit was obtained from Invitrogen. The molecular weight (M_{wv}) of nylon 6 was measured by viscosimetry, yielding a value of 22.5 ± 1 kDa. The following buffer solutions were prepared: 0.4 M sodium acetate buffer (pH 4–7) and 10 mM sodium borate buffer of pH 8.5. Fetal bovine serum (FBS) and Dulbecco's modified Eagle's medium (DMEM) were obtained from GIBCO, Life Technologies (Carlsbad, CA, USA).

3.2. Characterization of MNCs, NCs, and DOX-Loaded Nanosystems

The dynamic-light-scattering (DLS) and ζ -potential measurements were taken on a Malvern Zetasizer Nano device (Malvern Instruments, Worcestershire, UK) in aqueous media. Transmission electron microscopy (TEM) images were captured on a Jem-1400 (Jeol, Tokyo, Japan). Electronic absorption spectra were recorded on a UV-2100 spectrometer (Shimadzu, Kyoto, Japan) or microplate reader Clariostar (BMG, Ortenberg, Germany). The concentrations of DOX were determined by absorption at 480 nm using a calibration curve (Figure S2). FTIR spectra were measured on a 640-IR FT-IR spectrometer (Varian, MA, USA) from 4000 to 400 cm^{-1} at 25 °C accompanied with a KBr pellet.

3.3. MNP and MNP_OA Synthesis

The magnetic nanoparticles (MNPs) were synthesized according to the previously published Fe^{2+} and Fe^{3+} salt ($[\text{Fe}^{3+}]/[\text{Fe}^{2+}] = 2$) co-precipitation method [18,80]. The MNPs had average sizes of 11.0 ± 2.4 nm and 120 ± 5 nm as determined by TEM and DLS, respectively. There were no differences in the properties of the MNPs between this study and the published data [80].

The synthesis of OA-coated MNPs (MNP_OA) was carried out according to a previously published method [13]. The MNP_OA had an average size of 110 ± 15 nm as determined by DLS.

3.4. Synthesis of Nylon 6 Nanocomposites (MNP_Ny, MNP_OA_Ny)

Nylon-6 coating was performed in a 5 mL flask containing 300 μ L of MNPs or MNP_OA (1.13%), 2.5 mL of distilled ethyl alcohol, 0.2 μ L of mQ water, and 0.05% tween-20. The mixture was placed in an ultrasonic bath for 15 min. Then, 75 μ L of 28% aqueous ammonia solution and 10.5 μ L of tetraorthosilicate (TEOS) were added to the mixture with subsequent sonification in a “Sapphire” (Sapphire company, Moscow, Russia; ultrasonic frequency 35 kHz, 50 W) sonication bath for 15 min and stirred at 1500 rpm for 18 h at 25 °C. The nanocomposites were magnetically separated and washed three times with ethanol. A total of 150 μ L of 5% ethanol solution of aminopropyltriethoxysilane (APTES) was added to the precipitate and stirred at 1400 rpm for 2 h. Afterward, nanocomposites were magnetically separated and washed three times with ethanol and once with acetonitrile. A 3 mL solution of 1,3,5-trichloro-2,4,6-triazine (10 mg/mL) in acetonitrile was added to the precipitate and stirred at 1400 rpm for 2 h. Afterward, nanocomposites were magnetically separated and washed three times with acetonitrile and once with trifluoroethanol. A 4% solution of nylon-6 in trifluoroethanol/water mixture (80/20, *v/v*) was added to the surface-active nanocomposites of 10–15 mg/mL and incubated overnight under stirring (1400 rpm) at 25 °C. The MNP_Ny and MNP_OA_Ny were magnetically separated and washed three times with trifluoroethanol/water mixture (80/20, *v/v*), once with 50/50, 20/80 mixtures, and once with mQ water.

3.5. Synthesis of Nylon-6-Based Nanocapsules (NC1 and NC2)

The nanocapsules were synthesized via the incubation of MNP_Ny or MNP_OA_Ny with 3.5 M HCl at 90 °C for 60 min. The nanocapsules were separated by centrifugation, washed twice with mQ water, neutralized with 100 mM buffer (10 mM Tris-HCl, 50 mM KCl, 0.1% Tween-20, and 1.8 mM MgCl₂ at pH 9.5), and resuspended in mQ water.

3.6. DOX Loading

The DOX loading on 1 mg of MNCs or NCs was carried out in 1 mL of 10 mM sodium borate buffer (pH 8.5) containing the drug at 1 mg/mL concentration. The mixture was incubated at 25 °C for 12 h under stirring (700 rpm). Afterward, nanocomposites were separated via centrifugation (13,400 rpm, 5 min) and washed with 1 mL of buffer solution three times. The DOX concentration in the discarded solution was measured spectrophotometrically (480 nm, Figure S2, see Section 3.2). The bound drug amount was estimated as capacity E μ g/mg (DOX/MNCs or NCs) according to the equation: $E = (\text{DOX}_0 - \text{DOX})/N$. DOX_0 and DOX represent the initial and the discarded solution amounts of DOX (μ g), respectively. N denotes the amount of nanocomposites (mg).

3.7. DOX Release

DOX release was studied in 1 mL of 100 mM acetate buffer at pH ranging from 4 to 7 at 25 °C containing 1 mg of DOX-loaded MNCs or NCs under stirring (750 rpm). To determine the concentration of doxorubicin from the solutions, nanocomposites were separated by centrifugation (13,400 rpm, 5 min) and 100 μ L aliquots were taken at various periods and analyzed by UV-vis spectroscopy (480 nm, see Section 3.2). The amount of the released DOX was calculated using a serial dilution of a DOX standard solution (Figure S2).

4. Conclusions

In summary, nylon-6-coated magnetic nanocomposites and nanocapsules with a nylon-6 membrane were developed. The nylon-6-based polymer nanocapsules were obtained for the first time in the present work. This material is highly promising due to nylon-6's high biocompatibility. DLS, TEM, FTIR, and ζ -potential measurements were used for analyses of morphology, size, and charge. The TEM and DLS methods showed optimal sizes of the nano-constructions for drug delivery applications. The oleic-acid-coated nylon-6 MNCs and NCs showed excellent DOX loading values of up to 732 and 943 μ g/mg, respectively. On the contrary, the non-modified-with-oleic-acid nano-construction's capacity did not exceed

140 µg/mg. The proposed DOX-loaded MNCs and NCs provide pH-stimuli-responsive drug release properties, with the highest efficiency presented in acidic media. An MTT assay on the A549 and HEK 293FT cell lines demonstrated good cancer cell inhibition. Due to their suitable size, high DOX capacity, efficient drug release characteristics, and low IC₅₀ value, the oleic-acid-coated NC₂_DOX nano-constructions offer great prospects for cancer treatment.

Supplementary Materials: The following supporting information can be downloaded at: <https://www.mdpi.com/article/10.3390/magnetochemistry9040106/s1>. Figure S1: Scheme of the qualitative reaction of the nylon determination in MNP_OA_Ny (left) and MNP_OA (right) with N-(2-hydroxyethyl)-phenazinium ion. The reaction product is colored blue-violet in the presence of nylon. The initial MNP_OA was used as a control. Figure S2: Doxorubicin calibration curve for concentration calculation for adsorption or release studies by UV-vis. spectroscopy ($\lambda = 480$ nm). Figure S3: DOX-loaded NC₂ time-dependent drug release at various pH values. Figure S4: UV-vis spectra of aliquots in DOX-loaded NC₂ time-dependent drug release experiment at pH 6.

Author Contributions: Conceptualization, E.D.; methodology, E.D., A.C. and Y.Z.; investigation, E.K.; data curation, E.K. and Y.P.; writing—original draft preparation, A.C. and E.K.; writing—review and editing, E.D. and Y.Z.; project administration, A.C. and E.D.; funding acquisition, A.C. and E.D. All authors have read and agreed to the published version of the manuscript.

Funding: This study was funded by the Ministry of Science and Higher Education of the Russian Federation (state registration No. 121031300042-1).

Institutional Review Board Statement: Not applicable.

Informed Consent Statement: Not applicable.

Data Availability Statement: Not applicable.

Acknowledgments: We thank Kirillov V.L. (Borekov Institute of Catalysis SB RAS) for the fruitful discussion concerning MNP synthesis.

Conflicts of Interest: The authors declare no conflict of interest.

References

1. Eslami, P.; Albino, M.; Scavone, F.; Chiellini, F.; Morelli, A.; Baldi, G.; Cappiello, L.; Doumett, S.; Lorenzi, G.; Ravagli, C.; et al. Smart Magnetic Nanocarriers for Multi-Stimuli On-Demand Drug Delivery. *Nanomaterials* **2022**, *12*, 303. [CrossRef] [PubMed]
2. Carvalho, C.; Santos, R.; Cardoso, S.; Correia, S.; Oliveira, P.; Santos, M.; Moreira, P. Doxorubicin: The Good, the Bad and the Ugly Effect. *Curr. Med. Chem.* **2009**, *16*, 3267–3285. [CrossRef] [PubMed]
3. Radu, E.R.; Semenescu, A.; Voicu, S.I. Recent Advances in Stimuli-Responsive Doxorubicin Delivery Systems for Liver Cancer Therapy. *Polymers* **2022**, *14*, 5249. [CrossRef] [PubMed]
4. Sritharan, S.; Sivalingam, N. A comprehensive review on time-tested anticancer drug doxorubicin. *Life Sci.* **2021**, *278*, 119527. [CrossRef] [PubMed]
5. Christidi, E.; Brunham, L.R. Regulated cell death pathways in doxorubicin-induced cardiotoxicity. *Cell Death Dis.* **2021**, *12*, 339. [CrossRef] [PubMed]
6. Maruf, A.; Milewska, M.; Lalik, A.; Wandzik, I. pH and Reduction Dual-Responsive Nanogels as Smart Nanocarriers to Resist Doxorubicin Aggregation. *Molecules* **2022**, *27*, 5983. [CrossRef]
7. Curry, D.; Cameron, A.; MacDonald, B.; Nganou, C.; Scheller, H.; Marsh, J.; Beale, S.; Lu, M.; Shan, Z.; Kaliaperumal, R.; et al. Adsorption of doxorubicin on citrate-capped gold nanoparticles: Insights into engineering potent chemotherapeutic delivery systems. *Nanoscale* **2015**, *7*, 19611–19619. [CrossRef]
8. Popova, V.; Poletaeva, Y.; Pyshnaya, I.; Pyshnyi, D.; Dmitrienko, E. Designing pH-Dependent Systems Based on Nanoscale Calcium Carbonate for the Delivery of an Antitumor Drug. *Nanomaterials* **2021**, *11*, 2794. [CrossRef]
9. Yang, H.; Wang, N.; Yang, R.; Zhang, L.; Jiang, X. Folic acid-decorated β -cyclodextrin-based poly(ϵ -caprolactone)-dextran star polymer with disulfide bond-linker as theranostic nanoparticle for tumor-targeted mri and chemotherapy. *Pharmaceutics* **2022**, *14*, 52. [CrossRef]
10. Caldera, F.; Nisticò, R.; Magnacca, G.; Matencio, A.; Khazaei Monfared, Y.; Trotta, F. Magnetic Composites of Dextrin-Based Carbonate Nanosponges and Iron Oxide Nanoparticles with Potential Application in Targeted Drug Delivery. *Nanomaterials* **2022**, *12*, 754. [CrossRef]

11. Al-Musawi, S.; Albukhaty, S.; Al-Karagoly, H.; Almalki, F. Design and synthesis of multi-functional superparamagnetic core-gold shell coated with chitosan and folate nanoparticles for targeted antitumor therapy. *Nanomaterials* **2021**, *11*, 32. [[CrossRef](#)] [[PubMed](#)]
12. Carvalho, S.M.; Leonel, A.G.; Mansur, A.A.P.; Carvalho, I.C.; Krambrock, K.; Mansur, H.S. Bifunctional magnetopolymersomes of iron oxide nanoparticles and carboxymethylcellulose conjugated with doxorubicin for hyperthermo-chemotherapy of brain cancer cells. *Biomater. Sci.* **2019**, *7*, 2102–2122. [[CrossRef](#)] [[PubMed](#)]
13. Kovrigina, E.; Chubarov, A.; Dmitrienko, E. High Drug Capacity Doxorubicin-Loaded Iron Oxide Nanocomposites for Cancer Therapy. *Magnetochemistry* **2022**, *8*, 54. [[CrossRef](#)]
14. Awan, U.A.; Raza, A.; Ali, S.; Saeed, R.F.; Akhtar, N. Doxorubicin-loaded gold nanorods: A multifunctional chemo-photothermal nanoplatform for cancer management. *Beilstein J. Nanotechnol.* **2021**, *12*, 295–303. [[CrossRef](#)] [[PubMed](#)]
15. Mushtaq, S.; Shahzad, K.; Saeed, T.; Ul-Hamid, A.; Abbasi, B.H.; Ahmad, N.; Khalid, W.; Atif, M.; Ali, Z.; Abbasi, R. Biocompatibility and cytotoxicity in vitro of surface-functionalized drug-loaded spinel ferrite nanoparticles. *Beilstein J. Nanotechnol.* **2021**, *12*, 1339–1364. [[CrossRef](#)]
16. Popova, V.; Poletaeva, Y.; Chubarov, A.; Pyshnyi, D.; Dmitrienko, E. Doxorubicin-Loaded Silica Nanocomposites for Cancer Treatment. *Coatings* **2023**, *13*, 324. [[CrossRef](#)]
17. Popova, V.; Dmitrienko, E.; Chubarov, A. Magnetic Nanocomposites and Imprinted Polymers for Biomedical Applications of Nucleic Acids. *Magnetochemistry* **2023**, *9*, 12. [[CrossRef](#)]
18. Bulgakova, A.; Chubarov, A.; Dmitrienko, E. Magnetic Nylon 6 Nanocomposites for the Microextraction of Nucleic Acids from Biological Samples. *Magnetochemistry* **2022**, *8*, 85. [[CrossRef](#)]
19. Chubarov, A.S. Serum Albumin for Magnetic Nanoparticles Coating. *Magnetochemistry* **2022**, *8*, 13. [[CrossRef](#)]
20. Petrov, K.D.; Chubarov, A.S. Magnetite Nanoparticles for Biomedical Applications. *Encyclopedia* **2022**, *2*, 1811–1828. [[CrossRef](#)]
21. Popova, V.; Poletaeva, Y.; Chubarov, A.; Dmitrienko, E. pH-Responsible Doxorubicin-Loaded Fe₃O₄@CaCO₃ Nanocomposites for Cancer Treatment. *Pharmaceutics* **2023**, *15*, 771. [[CrossRef](#)] [[PubMed](#)]
22. Anderson, S.D.; Gwenin, V.V.; Gwenin, C.D. Magnetic Functionalized Nanoparticles for Biomedical, Drug Delivery and Imaging Applications. *Nanoscale Res. Lett.* **2019**, *14*, 188. [[CrossRef](#)] [[PubMed](#)]
23. Crețu, B.E.B.; Dodi, G.; Shavandi, A.; Gardikiotis, I.; Șerban, I.L.; Balan, V. Imaging constructs: The rise of iron oxide nanoparticles. *Molecules* **2021**, *26*, 3437. [[CrossRef](#)]
24. Anik, M.I.; Hossain, M.K.; Hossain, I.; Mahfuz, A.M.U.B.; Rahman, M.T.; Ahmed, I. Recent progress of magnetic nanoparticles in biomedical applications: A review. *Nano Sel.* **2021**, *2*, 1146–1186. [[CrossRef](#)]
25. Comanescu, C. Magnetic Nanoparticles: Current Advances in Nanomedicine, Drug Delivery and MRI. *Chemistry* **2022**, *4*, 872–930. [[CrossRef](#)]
26. Włodarczyk, A.; Gorgoń, S.; Radoń, A.; Bajdak-Rusinek, K. Magnetite Nanoparticles in Magnetic Hyperthermia and Cancer Therapies: Challenges and Perspectives. *Nanomaterials* **2022**, *12*, 1807. [[CrossRef](#)]
27. Materón, E.M.; Miyazaki, C.M.; Carr, O.; Joshi, N.; Picciani, P.H.S.; Dalmascio, C.J.; Davis, F.; Shimizu, F.M. Magnetic nanoparticles in biomedical applications: A review. *Appl. Surf. Sci. Adv.* **2021**, *6*, 100163. [[CrossRef](#)]
28. Bobrikova, E.; Chubarov, A.; Dmitrienko, E. The Effect of pH and Buffer on Oligonucleotide Affinity for Iron Oxide Nanoparticles. *Magnetochemistry* **2021**, *7*, 128. [[CrossRef](#)]
29. Zheng, R.; Guo, J.; Cai, X.; Bin, L.; Lu, C.; Singh, A.; Trivedi, M.; Kumar, A.; Liu, J. Manganese complexes and manganese-based metal-organic frameworks as contrast agents in MRI and chemotherapeutics agents: Applications and prospects. *Colloids Surf. B Biointerfaces* **2022**, *213*, 112432. [[CrossRef](#)]
30. Li, C.; Chen, T.; Ocoy, I.; Zhu, G.; Yasun, E.; You, M.; Wu, C.; Zheng, J.; Song, E.; Huang, C.Z.; et al. Gold-Coated Fe₃O₄ nanoroses with five unique functions for cancer cell targeting, imaging, and therapy. *Adv. Funct. Mater.* **2014**, *24*, 1772–1780. [[CrossRef](#)]
31. Shen, S.; Wu, L.; Liu, J.; Xie, M.; Shen, H.; Qi, X.; Yan, Y.; Ge, Y.; Jin, Y. Core-shell structured Fe₃O₄@TiO₂-doxorubicin nanoparticles for targeted chemo-sonodynamic therapy of cancer. *Int. J. Pharm.* **2015**, *486*, 380–388. [[CrossRef](#)] [[PubMed](#)]
32. Lamichhane, N.; Sharma, S.; Parul, Verma, A.K.; Roy, I.; Sen, T. Iron oxide-based magneto-optical nanocomposites for in vivo biomedical applications. *Biomedicines* **2021**, *9*, 288. [[CrossRef](#)] [[PubMed](#)]
33. Chouhan, R.S.; Horvat, M.; Ahmed, J.; Alhokbany, N.; Alshehri, S.M.; Gandhi, S. Magnetic nanoparticles—A multifunctional potential agent for diagnosis and therapy. *Cancers* **2021**, *13*, 2213. [[CrossRef](#)] [[PubMed](#)]
34. Shabatina, T.I.; Vernaya, O.I.; Shabatina, V.P.; Melnikov, M.Y. Magnetic nanoparticles for biomedical purposes: Modern trends and prospects. *Magnetochemistry* **2020**, *6*, 30. [[CrossRef](#)]
35. Hepel, M. Magnetic nanoparticles for nanomedicine. *Magnetochemistry* **2020**, *6*, 3. [[CrossRef](#)]
36. Dulińska-Litewka, J.; Łazarczyk, A.; Hałubiec, P.; Szafranski, O.; Karnas, K.; Karewicz, A. Superparamagnetic iron oxide nanoparticles-current and prospective medical applications. *Materials* **2019**, *12*, 617. [[CrossRef](#)] [[PubMed](#)]
37. Stueber, D.D.; Villanova, J.; Aponte, I.; Xiao, Z. Magnetic Nanoparticles in Biology and Medicine: Past, Present, and Future Trends. *Pharmaceutics* **2021**, *13*, 943. [[CrossRef](#)]
38. Socoliuc, V.; Peddis, D.; Petrenko, V.I.; Avdeev, M.V.; Susan-Resiga, D.; Szabó, T.; Turcu, R.; Tombác, E.; Vékás, L. Magnetic nanoparticle systems for nanomedicine—A materials science perspective. *Magnetochemistry* **2020**, *6*, 2. [[CrossRef](#)]
39. Bruschi, M.L.; de Toledo, L.D.A.S. Pharmaceutical applications of iron-oxide magnetic nanoparticles. *Magnetochemistry* **2019**, *5*, 50. [[CrossRef](#)]

40. Singh, N.; Sallem, F.; Mirjolet, C.; Nury, T.; Sahoo, S.K.; Millot, N.; Kumar, R. Polydopamine modified superparamagnetic iron oxide nanoparticles as multifunctional nanocarrier for targeted prostate cancer treatment. *Nanomaterials* **2019**, *9*, 138. [[CrossRef](#)]
41. Popescu, R.C.; Savu, D.; Dorobantu, I.; Vasile, B.S.; Hosser, H.; Boldeiu, A.; Temelie, M.; Straticiuc, M.; Iancu, D.A.; Andronescu, E.; et al. Efficient uptake and retention of iron oxide-based nanoparticles in HeLa cells leads to an effective intracellular delivery of doxorubicin. *Sci. Rep.* **2020**, *10*, 10530. [[CrossRef](#)] [[PubMed](#)]
42. Popescu, R.C.; Savu, D.I.; Bierbaum, M.; Grbenicek, A.; Schneider, F.; Hosser, H.; Vasile, B.S.; Andronescu, E.; Wenz, F.; Giordano, F.A.; et al. Intracellular delivery of doxorubicin by iron oxide-based nano-constructs increases clonogenic inactivation of ionizing radiation in hela cells. *Int. J. Mol. Sci.* **2021**, *22*, 6778. [[CrossRef](#)] [[PubMed](#)]
43. Piehler, S.; Dähring, H.; Grandke, J.; Göring, J.; Couleaud, P.; Aires, A.; Cortajarena, A.L.; Courty, J.; Latorre, A.; Somoza, Á.; et al. Iron oxide nanoparticles as carriers for DOX and magnetic hyperthermia after intratumoral application into breast cancer in mice: Impact and future perspectives. *Nanomaterials* **2020**, *10*, 1016. [[CrossRef](#)] [[PubMed](#)]
44. Norouzi, M.; Yathindranath, V.; Thliveris, J.A.; Kopec, B.M.; Siahaan, T.J.; Miller, D.W. Doxorubicin-loaded iron oxide nanoparticles for glioblastoma therapy: A combinational approach for enhanced delivery of nanoparticles. *Sci. Rep.* **2020**, *10*, 11292. [[CrossRef](#)]
45. Khaleedian, M.; Nourbakhsh, M.S.; Saber, R.; Hashemzadeh, H.; Darvishi, M.H. Preparation and evaluation of doxorubicin-loaded pla-peg-fa copolymer containing superparamagnetic iron oxide nanoparticles (Spions) for cancer treatment: Combination therapy with hyperthermia and chemotherapy. *Int. J. Nanomed.* **2020**, *15*, 6167–6182. [[CrossRef](#)]
46. Shen, C.; Wang, X.; Zheng, Z.; Gao, C.; Chen, X.; Zhao, S.; Dai, Z. Doxorubicin and indocyanine green loaded superparamagnetic iron oxide nanoparticles with PEGylated phospholipid coating for magnetic resonance with fluorescence imaging and chemotherapy of glioma. *Int. J. Nanomed.* **2019**, *14*, 101–117. [[CrossRef](#)]
47. Nieciecka, D.; Celej, J.; Żuk, M.; Majkowska-pilip, A.; Żelechowska-matysiak, K.; Lis, A.; Osial, M. Hybrid system for local drug delivery and magnetic hyperthermia based on spions loaded with doxorubicin and epirubicin. *Pharmaceutics* **2021**, *13*, 480. [[CrossRef](#)]
48. Nogueira, J.; Soares, S.F.; Amorim, C.O.; Amaral, J.S.; Silva, C.; Martel, F.; Trindade, T.; Daniel-Da-Silva, A.L. Magnetic driven nanocarriers for pH-responsive doxorubicin release in cancer therapy. *Molecules* **2020**, *25*, 333. [[CrossRef](#)]
49. Darwish, M.S.A.; Mostafa, M.H.; Al-Harbi, L.M. Polymeric Nanocomposites for Environmental and Industrial Applications. *Int. J. Mol. Sci.* **2022**, *23*, 1023. [[CrossRef](#)]
50. Mukhopadhyay, A.; Joshi, N.; Chattopadhyay, K.; De, G. A facile synthesis of PEG-coated magnetite (Fe₃O₄) nanoparticles and their prevention of the reduction of cytochrome C. *ACS Appl. Mater. Interfaces* **2012**, *4*, 142–149. [[CrossRef](#)]
51. Huang, Y.; Zhang, B.; Xie, S.; Yang, B.; Xu, Q.; Tan, J. Superparamagnetic Iron Oxide Nanoparticles Modified with Tween 80 Pass through the Intact Blood-Brain Barrier in Rats under Magnetic Field. *ACS Appl. Mater. Interfaces* **2016**, *8*, 11336–11341. [[CrossRef](#)] [[PubMed](#)]
52. Yoon, H.M.; Kang, M.S.; Choi, G.E.; Kim, Y.J.; Bae, C.H.; Yu, Y.B.; Jeong, Y. II Stimuli-responsive drug delivery of doxorubicin using magnetic nanoparticle conjugated poly(Ethylene glycol)-g-chitosan copolymer. *Int. J. Mol. Sci.* **2021**, *22*, 13169. [[CrossRef](#)] [[PubMed](#)]
53. Snoderly, H.T.; Freshwater, K.A.; Martinez de la Torre, C.; Panchal, D.M.; Vito, J.N.; Bennewitz, M.F. PEGylation of Metal Oxide Nanoparticles Modulates Neutrophil Extracellular Trap Formation. *Biosensors* **2022**, *12*, 123. [[CrossRef](#)] [[PubMed](#)]
54. Mylkie, K.; Nowak, P.; Rybczynski, P.; Ziegler-Borowska, M. Polymer-coated magnetite nanoparticles for protein immobilization. *Materials* **2021**, *14*, 248. [[CrossRef](#)] [[PubMed](#)]
55. Jabir, M.S.; Nayef, U.M.; Kadhim, W.K.A. Polyethylene Glycol-Functionalized Magnetic (Fe₃O₄) Nanoparticles: A Novel DNA-Mediated Antibacterial Agent. *Nano Biomed. Eng.* **2019**, *11*, 18–27. [[CrossRef](#)]
56. Gómez-Vallejo, V.; Puigvila, M.; Plaza-García, S.; Szczupak, B.; Piñol, R.; Murillo, J.L.; Sorribas, V.; Lou, G.; Veintemillas, S.; Ramos-Cabrer, P.; et al. PEG-copolymer-coated iron oxide nanoparticles that avoid the reticuloendothelial system and act as kidney MRI contrast agents. *Nanoscale* **2018**, *10*, 14153–14164. [[CrossRef](#)]
57. Shen, L.; Li, B.; Qiao, Y. Fe₃O₄ nanoparticles in targeted drug/gene delivery systems. *Materials* **2018**, *11*, 324. [[CrossRef](#)]
58. Jiao, W.; Zhang, T.; Peng, M.; Yi, J.; He, Y.; Fan, H. Design of Magnetic Nanoplatforms for Cancer Theranostics. *Biosensors* **2022**, *12*, 38. [[CrossRef](#)] [[PubMed](#)]
59. Ayub, A.; Wettig, S. An Overview of Nanotechnologies for Drug Delivery to the Brain. *Pharmaceutics* **2022**, *14*, 224. [[CrossRef](#)]
60. Kadhim, W.K.A.; Nayef, U.M.; Jabir, M.S. Polyethylene glycol-functionalized magnetic (Fe₃O₄) nanoparticles: A good method for a successful antibacterial therapeutic agent via damage DNA molecule. *Surf. Rev. Lett.* **2019**, *26*. [[CrossRef](#)]
61. Shakiba, M.; Rezvani Ghomi, E.; Khosravi, F.; Jouybar, S.; Bigham, A.; Zare, M.; Abdouss, M.; Moaref, R.; Ramakrishna, S. Nylon—A material introduction and overview for biomedical applications. *Polym. Adv. Technol.* **2021**, *32*, 3368–3383. [[CrossRef](#)]
62. Reyes-Gallardo, E.M.; Lucena, R.; Cárdenas, S. Silica nanoparticles-nylon 6 composites: Synthesis, characterization and potential use as sorbent. *RSC Adv.* **2017**, *7*, 2308–2314. [[CrossRef](#)]
63. Mahfuz, H.; Hasan, M.; Dhanak, V.; Beamson, G.; Stewart, J.; Rangari, V.; Wei, X.; Khabashesku, V.; Jeelani, S. Reinforcement of nylon 6 with functionalized silica nanoparticles for enhanced tensile strength and modulus. *Nanotechnology* **2008**, *19*, 445702. [[CrossRef](#)]
64. Mateos-Maroto, A.; Fernández-Peña, L.; Abelenda-Núñez, I.; Ortega, F.; Rubio, R.G.; Guzmán, E. Polyelectrolyte Multilayered Capsules as Biomedical Tools. *Polymers* **2022**, *14*, 479. [[CrossRef](#)] [[PubMed](#)]

65. Balan, V.; Dodi, G.; Tudorachi, N.; Ponta, O.; Simon, V.; Butnaru, M.; Verestiuc, L. Doxorubicin-loaded magnetic nanocapsules based on N-palmitoyl chitosan and magnetite: Synthesis and characterization. *Chem. Eng. J.* **2015**, *279*, 188–197. [[CrossRef](#)]
66. Poletto, F.S.; Beck, R.C.R.; Guterres, S.S.; Pohlmann, A.R. Polymeric Nanocapsules: Concepts and Applications. In *Nanocosmetics and Nanomedicines*; Springer: Berlin/Heidelberg, Germany, 2011; pp. 49–68, ISBN 9789896540821.
67. Fahmi, A.; Abdur-Rahman, M.; Mahareek, O.; Shemis, M.A. Synthesis, characterization, and cytotoxicity of doxorubicin-loaded polycaprolactone nanocapsules as controlled anti-hepatocellular carcinoma drug release system. *BMC Chem.* **2022**, *16*, 1–15. [[CrossRef](#)]
68. Sharma, V.; Vijay, J.; Ganesh, M.R.; Sundaramurthy, A. Multilayer capsules encapsulating nimbin and doxorubicin for cancer chemo-photothermal therapy. *Int. J. Pharm.* **2020**, *582*, 119350. [[CrossRef](#)]
69. Milosavljevic, V.; Jamroz, E.; Gagic, M.; Haddad, Y.; Michalkova, H.; Balkova, R.; Tesarova, B.; Moulick, A.; Heger, Z.; Richtera, L.; et al. Encapsulation of Doxorubicin in Furcellaran/Chitosan Nanocapsules by Layer-by-Layer Technique for Selectively Controlled Drug Delivery. *Biomacromolecules* **2020**, *21*, 418–434. [[CrossRef](#)]
70. Razzaque, S.; Cheng, Y.; Hussain, I.; Tan, B. Synthesis of surface functionalized hollow microporous organic capsules for doxorubicin delivery to cancer cells. *Polym. Chem.* **2020**, *11*, 2110–2118. [[CrossRef](#)]
71. Kucharczyk, K.; Florczak, A.; Deptuch, T.; Penderecka, K.; Jastrzebska, K.; Mackiewicz, A.; Dams-Kozłowska, H. Drug affinity and targeted delivery: Double functionalization of silk spheres for controlled doxorubicin delivery into Her2-positive cancer cells. *J. Nanobiotechnol.* **2020**, *18*, 1–13. [[CrossRef](#)]
72. Trushina, D.B.; Akasov, R.A.; Khovankina, A.V.; Borodina, T.N.; Bukreeva, T.V.; Markvicheva, E.A. Doxorubicin-loaded biodegradable capsules: Temperature induced shrinking and study of cytotoxicity in vitro. *J. Mol. Liq.* **2019**, *284*, 215–224. [[CrossRef](#)]
73. Shen, H.; Li, F.; Wang, D.; Yang, Z.; Yao, C.; Ye, Y.; Wang, X. Chitosan-alginate BSA-gel-capsules for local chemotherapy against drug-resistant breast cancer. *Drug Des. Dev. Ther.* **2018**, *12*, 921–934. [[CrossRef](#)] [[PubMed](#)]
74. Kato, Y.; Ozawa, S.; Miyamoto, C.; Maehata, Y.; Suzuki, A.; Maeda, T.; Baba, Y. Acidic extracellular microenvironment and cancer. *Cancer Cell Int.* **2013**, *13*, 89. [[CrossRef](#)] [[PubMed](#)]
75. Santhamoorthy, M.; Vy Phan, T.T.; Ramkumar, V.; Raorane, C.J.; Thirupathi, K.; Kim, S.C. Thermo-Sensitive Poly (N-isopropylacrylamide-co-polyacrylamide) Hydrogel for pH-Responsive Therapeutic Delivery. *Polymers* **2022**, *14*, 4128. [[CrossRef](#)]
76. Ding, H.; Inoue, S.; Ljubimov, A.V.; Patil, R.; Portilla-Arias, J.; Hu, J.; Konda, B.; Wawrowsky, K.A.; Fujita, M.; Karabalin, N.; et al. Inhibition of brain tumor growth by intravenous poly (β -L-malic acid) nanobioconjugate with pH-dependent drug release. *Proc. Natl. Acad. Sci. USA* **2010**, *107*, 18143–18148. [[CrossRef](#)]
77. Dong, Z.; Feng, L.; Zhu, W.; Sun, X.; Gao, M.; Zhao, H.; Chao, Y.; Liu, Z. CaCO₃ nanoparticles as an ultra-sensitive tumor-pH-responsive nanoplatfrom enabling real-time drug release monitoring and cancer combination therapy. *Biomaterials* **2016**, *110*, 60–70. [[CrossRef](#)]
78. Mahdavinia, G.R.; Hoseinzadeh, H.; Labib, P.; Jabbari, P.; Mohebbi, A.; Barzegar, S.; Jafari, H. (Magnetic laponite/ κ -carrageenan)/chitosan core-shell carrier for pH-sensitive release of doxorubicin. *Polym. Bull.* **2023**. [[CrossRef](#)]
79. Ahmad, I.; Khan, M.F.A.; Rahdar, A.; Hussain, S.; Tareen, F.K.; Salim, M.W.; Ajalli, N.; Amirzada, M.I.; Khan, A. Design and Evaluation of pH Sensitive PEG-Protamine Nanocomplex of Doxorubicin for Treatment of Breast Cancer. *Polymers* **2022**, *14*, 2403. [[CrossRef](#)]
80. Kirillov, V.L.; Balaev, D.A.; Semenov, S.V.; Shaikhutdinov, K.A.; Martyanov, O.N. Size control in the formation of magnetite nanoparticles in the presence of citrate ions. *Mater. Chem. Phys.* **2014**, *145*, 75–81. [[CrossRef](#)]
81. Mahdavi, M.; Bin Ahmad, M.; Haron, M.J.; Namvar, F.; Nadi, B.; Ab Rahman, M.Z.; Amin, J. Synthesis, surface modification and characterisation of biocompatible magnetic iron oxide nanoparticles for biomedical applications. *Molecules* **2013**, *18*, 7533–7548. [[CrossRef](#)]
82. Yallapu, M.M.; Foy, S.P.; Jain, T.K.; Labhasetwar, V. PEG-functionalized magnetic nanoparticles for drug delivery and magnetic resonance imaging applications. *Pharm. Res.* **2010**, *27*, 2283–2295. [[CrossRef](#)] [[PubMed](#)]
83. Ching, Y.C.; Gunathilake, T.M.S.U.; Chuah, C.H.; Ching, K.Y.; Singh, R.; Liou, N.S. Curcumin/Tween 20-incorporated cellulose nanoparticles with enhanced curcumin solubility for nano-drug delivery: Characterization and in vitro evaluation. *Cellulose* **2019**, *26*, 5467–5481. [[CrossRef](#)]
84. Clavijo, C.; Osma, J.F. Functionalized leather: A novel and effective hazardous solid waste adsorbent for the removal of the diazo dye congo red from aqueous solution. *Water* **2019**, *11*, 1906. [[CrossRef](#)]
85. Wang, Y.; Sun, Y.; Wang, J.; Yang, Y.; Li, Y.; Yuan, Y.; Liu, C. Charge-Reversal APTES-Modified Mesoporous Silica Nanoparticles with High Drug Loading and Release Controllability. *Appl. Mater. Interfaces* **2016**, *8*, 17166–17175. [[CrossRef](#)]
86. Digigow, R.G.; Dechézelles, J.; Dietsch, H.; Geissbühler, I.; Vanhecke, D.; Geers, C.; Hirt, A.M.; Rothen-rutishauser, B. Preparation and characterization of functional silica hybrid magnetic nanoparticles. *J. Magn. Magn. Mater.* **2014**, *362*, 72–79. [[CrossRef](#)]
87. Chandra, S.; Beaune, G.; Shirahata, N.; Winnik, F.M. A one-pot synthesis of water soluble highly fluorescent silica nanoparticles. *J. Mater. Chem. B* **2017**, *5*, 1363. [[CrossRef](#)]
88. Ismail, A.F.; Goh, P.; Rezaei, M.; Arzhandi, D.; Ismail, N. Aptes and teos modified binary recyclable hybrid Fe₃O₄@GO nanocomposite for photocatalytic dye removal. *J. Teknol.* **2018**, *80*, 157–164. [[CrossRef](#)]
89. Hao, N.; Jayawardana, K.W.; Chen, X.; Zoysa, T.D.; Yan, M. One-step synthesis of amine-functionalized hollow mesoporous silica nanoparticles as efficient antibacterial and anticancer materials. *ACS Appl Mater Interfaces* **2015**, *7*, 1040–1045. [[CrossRef](#)]

90. Chacón-Torres, J.C.; Reinoso, C.; Navas-León, D.G.; Briceño, S.; González, G. Optimized and scalable synthesis of magnetic nanoparticles for RNA extraction in response to developing countries' needs in the detection and control of SARS-CoV-2. *Sci. Rep.* **2020**, *10*, 19004. [[CrossRef](#)]
91. Ibarra, J.; Melendres, J.; Almada, M.; Burboa, M.G.; Taboada, P.; Juárez, J.; Valdez, M.A. Synthesis and characterization of magnetite/PLGA/chitosan nanoparticles. *Mater. Res. Express* **2015**, *2*, 95010. [[CrossRef](#)]
92. Wang, C.; Yan, J.; Cui, X.; Cong, D.; Wang, H. Preparation and characterization of magnetic hollow PMMA nanospheres via in situ emulsion polymerization. *Colloids Surfaces Physicochem. Eng. Asp.* **2010**, *363*, 71–77. [[CrossRef](#)]
93. Kowalik, P.; Elbaum, D.; Mikulski, J.; Fronc, K.; Kamińska, I.; Morais, P.C.; Eduardo De Souza, P.; Nunes, R.B.; Veiga-Souza, F.H.; Gruzel, G.; et al. Upconversion fluorescence imaging of HeLa cells using ROS generating SiO₂-coated lanthanide-doped NaYF₄ nanoconstructs. *RSC Adv.* **2017**, *7*, 30262–30273. [[CrossRef](#)]
94. Yang, K.; Peng, H.; Wen, Y.; Li, N. Re-examination of characteristic FTIR spectrum of secondary layer in bilayer oleic acid-coated Fe₃O₄ nanoparticles. *Appl. Surf. Sci.* **2010**, *256*, 3093–3097. [[CrossRef](#)]
95. Do, B.P.H.; Nguyen, B.D.; Nguyen, H.D.; Nguyen, P.T. Synthesis of magnetic composite nanoparticles enveloped in copolymers specified for scale inhibition application. *Adv. Nat. Sci. Nanosci. Nanotechnol.* **2013**, *4*, 45016. [[CrossRef](#)]
96. Stoia, M.; Istrate, R.; Păcurariu, C. Investigation of magnetite nanoparticles stability in air by thermal analysis and FTIR spectroscopy. *J. Therm. Anal. Calorim.* **2016**, *125*, 1185–1198. [[CrossRef](#)]
97. Vasanthan, N. Crystallinity determination of nylon 66 by density measurement and fourier transform infrared (FTIR) spectroscopy. *J. Chem. Educ.* **2012**, *89*, 387–390. [[CrossRef](#)]
98. Mahdi, H.A. An FTIR Study of Characterization of Neat and UV Stabilized Nylon 6,6 Polymer Films. *J. Pure Appl. Sci.* **2011**, *24*, 86–90.
99. Khor, N.K.E.M.; Salmiati; Hadibarata, T.; Yusop, Z. A combination of waste biomass activated carbon and nylon nanofiber for removal of triclosan from aqueous solutions. *J. Environ. Treat. Tech.* **2020**, *8*, 1036–1045. [[CrossRef](#)]
100. Al-Nadaf, A.H.; Dahabiyeh, L.A.; Jawarneh, S.; Bardaweel, S.; Mahmoud, N.N. Folic acid-hydrophilic polymer coated mesoporous silica nanoparticles target doxorubicin delivery. *Pharm. Dev. Technol.* **2021**, *26*, 582–591. [[CrossRef](#)]
101. Hao, N.; Li, L.; Zhang, Q.; Huang, X.; Meng, X.; Zhang, Y.; Chen, D.; Tang, F.; Li, L. The shape effect of PEGylated mesoporous silica nanoparticles on cellular uptake pathway in HeLa cells. *Microporous Mesoporous Mater.* **2012**, *162*, 14–23. [[CrossRef](#)]
102. Denisov, A.Y.; Pyshnyi, D.V.; Ivanova, E.M. The nature of stabilization of the tandem DNA duplex pTGGAGCTG · (pCAGC + (Phn-NH-(CH₂)₃-NH)pTCCA) basing on the UV, CD, and two-dimensional NMR spectroscopy data. *Russ. J. Bioorgan. Chem.* **2000**, *26*, 337–349. [[CrossRef](#)]
103. Pochapski, D.J.; Carvalho Dos Santos, C.; Leite, G.W.; Pulcinelli, S.H.; Santilli, C.V. Zeta Potential and Colloidal Stability Predictions for Inorganic Nanoparticle Dispersions: Effects of Experimental Conditions and Electrokinetic Models on the Interpretation of Results. *Langmuir* **2021**, *37*, 13379–13389. [[CrossRef](#)] [[PubMed](#)]
104. Gupta, R.; Pancholi, K.; De Sa, R.; Murray, D.; Huo, D.; Droubi, G.; White, M.; Njuguna, J. Effect of Oleic Acid Coating of Iron Oxide Nanoparticles on Properties of Magnetic Polyamide-6 Nanocomposite. *JOM* **2019**, *71*, 3119–3128. [[CrossRef](#)]

Disclaimer/Publisher's Note: The statements, opinions and data contained in all publications are solely those of the individual author(s) and contributor(s) and not of MDPI and/or the editor(s). MDPI and/or the editor(s) disclaim responsibility for any injury to people or property resulting from any ideas, methods, instructions or products referred to in the content.